Tunnelling and Underground Space Technology 157 (2025) 106318

Contents lists available at ScienceDirect

Tunnelling and Underground Space Technology incorporating Trenchless Technology Research

journal homepage: www.elsevier.com/locate/tust

Comparative study on seismic response of a shallow buried underground structure in coral sand and coral gravelly sand by centrifuge modeling

Zhongxiang Zhang [a], Su Chen [a,*], Yongzhi Wang [c], Xiaojun Li [a,b]

[a] Beijing University of Technology, Beijing 100124, China
[b] Institute of Geophysics, China Earthquake Administration, Beijing 100081, China
[c] Institute of Engineering Mechanics, China Earthquake Administration, Harbin 150080, China

ARTICLE INFO

Keywords:
Coral sand
Coral gravelly sand
Underground structure
Centrifuge shaking table tests
Seismic response

ABSTRACT

Coral sand, as a geological material for foundation filling, is widely used for reclamation projects in coral reef areas. The coral sand is characterized by a wide grain size distribution. A series of centrifuge shaking table tests were conducted to explore the seismic response of a shallow buried underground structure in saturated coral sand and coral gravelly sand. The emphasis was placed on comparing the similarities and differences in the dynamic behavior of the underground structure at the two sites. The responses of excess pore pressure, acceleration, displacement, and dynamic soil pressure of the structure were analyzed in detail. The results indicated that the underground structure in coral sand had a significant influence on the development of excess pore pressure in the surrounding soil, but this effect was not evident in coral gravelly sand due to well-drained channels. Liquefaction was observed in the soil layer around the structure in coral sand, but it did not occur in coral gravelly sand. In coral sand, the liquefaction of the soil layer at the bottom of the structure caused a significant attenuation in the acceleration of the structure. Compared to coral gravelly sand, the acceleration response of the soil layer near the bottom of the underground structure was higher in coral sand. During the shaking, the displacement pattern of the structure in coral gravelly sand was slight subsidence-slight uplift-significant subsidence, while it exhibited a significant uplift in coral sand. The maximum dynamic soil pressure distribution on the structural sidewalls presented a trapezoidal distribution, and the dynamic soil pressure had a strong connection with the development of excess pore pressure in the surrounding soil.

1. Introduction

Coral sand, primarily composed of the skeletal remains of corals, shells, and other marine organisms, can be found extensively in coral island reefs and seashores situated between 30 degrees north latitude and 30 degrees south latitude (Burke et al., 2011). With the advancement of marine engineering, land reclamation is increasingly being utilized for the construction or enhancement of port infrastructure and for filling construction sites (Sengupta et al., 2018). Coral sand is increasingly being utilized as a construction material for land reclamation projects in coral reef regions. However, these engineering sites are inevitably subjected to natural loads such as waves and earthquakes. Existing damage surveys have reported that the foundation and infrastructure at coral sand sites have suffered severe damage during earthquakes (Mejia and Yeung, 1995; Chock et al., 2006; Green et al., 2011; Olson et al., 2011).

The seismic behavior of structures at coral sand sites has attracted the attention of many scholars. Liu et al. (2020) studied the dynamic response of block-type quay walls at coral sand backfill sites and found that the seismic ability of block-type quay walls can be improved by increasing the density, permeability, and connection between blocks. Wu et al. (2020) compared the differences in seismic response of superstructure supported by pile groups at coral sand sites and siliceous sand sites through shaking table tests. The findings revealed that the horizontal displacement of the superstructure and the bending moment of the columns and piles at the coral sand site were less than those at the siliceous sand site. Through numerical simulations, Wu et al. (2021) reported that increasing the length of the piles in coral sand amplified the seismic response of the soil, but it reduced the settlement of the superstructure. The groundwater level had a significant influence on the seismic performance of a coral sand foundation–superstructure system and the rise in groundwater level could lead to an increase in both the

* Corresponding author.
E-mail address: chensuchina@126.com (S. Chen).

https://doi.org/10.1016/j.tust.2024.106318
Received 8 July 2024; Received in revised form 22 October 2024; Accepted 5 December 2024

settlement and horizontal displacements of the model structure (Ding et al., 2022). Zhang et al. (2022) explored the seismic response of the revetment breakwaters and nearby aircraft runways built on reclaimed lands with coral sand and found that the seismic stability of seawalls and airport runways was more adversely affected by loose coral sand foundations.

Given the limited land resources of island reefs, it is crucial to develop underground spaces. However, recent seismic events have reported severe damage to underground structures caused by strong seismic motions (Iida et al., 1996; Ghasemi et al., 2000; Wang et al., 2001, 2009; Yamaguchi et al., 2012; Moss et al., 2015; Wham et al., 2017; Hazarika et al., 2017). Some researchers have already conducted studies on the seismic response of underground structures in coral sand foundations. Ding et al. (2021) conducted a series of shaking table tests to investigate the effect of groundwater levels on the seismic response of an underground structure. The results illustrated that the settlement of the structure decreased with the increase in the groundwater level. The nonlinearity of coral sand near the groundwater level had a great influence on the seismic stability of underground structures during strong earthquakes and increasing the relative density of the coral sand foundation led to an increase in the horizontal dynamic soil pressure of the underground structure (Wu et al., 2023, 2024).

However, the maximum grain size of the sand at coral sand sites studied above did not exceed 2 mm. Reclaimed foundations on island reefs are characterized by a wide grain size distribution, which can be divided into coral sand sites and coral gravelly sand sites (Yuan et al., 2019; Wang et al., 2021; Wang et al., 2021; Gao and Ye, 2023). Few researches concern the seismic response of underground structures at coral gravelly sand sites. The content of gravel particles has a significant influence on the liquefaction behavior of saturated sand sites. Evans and Zhou (1995) conducted a series of undrained cyclic triaxial tests on sand-gravel composite specimens with different gravel contents. The findings revealed that the cyclic resistance increased with the increase in the gravel content. Ruttithivaphanich and Sasanakul (2022), Hubler (2017), and Xu et al. (2019) reached similar conclusions. Therefore, it is crucial to conduct a comparative study on the similarities and differences in the dynamic behavior of the underground structure in coral sand and coral gravelly sand.

This study conducted two centrifuge shaking table tests to explore the seismic response of a shallow buried underground structure in coral sand and coral gravelly sand. The differences and similarities in the development of excess pore pressure, acceleration response, vertical displacement pattern, and dynamic soil pressure of the underground structure were thoroughly compared. It provided a reference for the engineering practice at island reefs.

2. Experimental scheme

2.1. Centrifuge test apparatus

The experiments were carried out at a centrifugal acceleration of 50g using the DCIEM-40–300 centrifuge and a unidirectional shaking table at the Institute of Engineering Mechanics, China Earthquake Administration. The parameters of the centrifuge shaking table apparatus are listed in Table 1. A rigid container with a steel partition plate in the middle was employed in the tests. The internal dimensions of the container are 78 cm (length) × 58 cm (width) × 60 cm (height) and 52 cm (length) × 58 cm (width) × 60 cm (height) in model scale. Rigid containers are commonly utilized in centrifuge shaking table experiments (Yu et al., 2015; Wang et al., 2017; Zhou et al., 2018; Xie et al., 2021; Fan et al., 2023). Along the direction perpendicular to the shaking, a 4 cm thick piece of polystyrene foam board was attached to the inner walls of the container to minimize the potential boundary effect (Fig. 2(a)). The scaling laws are listed in Table 2.

Table 1
The parameters of the centrifuge shaking table apparatus.

Parameters	Values
Effective radius	5 m
Dynamic bearing capacity	1500 kg
Max. dynamic centrifugal acceleration	50 g
Max. shaking acceleration	30 g
Max. shaking velocity	± 1 m/s
Max. shaking displacement	± 15 mm
Shaking frequency	10–300 Hz
Payload area (length × width)	1.6 m × 0.8 m

2.2. Test materials

The experimental sand was collected from the reclaimed land of a certain island reef. Fig. 1 shows the grain size distribution curves of the test soil, which were determined based on the gradations in earlier research (Wang et al., 2021; Gao and Ye, 2023). According to the Chinese National Standard for Classification of Soils (GB/T50145-2007) (Chinese Ministry of Water Resources, 2007), the experimental sand can be classified as coral sand and coral gravelly sand. The basic properties of the test sand are presented in Table 3, determined using the ASTM D4253-14 and D4254-14 standards (ASTM, 2016a, 2016b).

The model underground structure was made of aluminum alloy material ($\rho = 2800$ kg/m^3), which has a density similar to that of reinforced concrete. The cross-sectional dimensions of the model structure are 150 mm (width) × 100 mm (height) × 15 mm (thickness) (Fig. 2(c)). The end of the model structure was sealed with a 3 mm thick acrylic sheet. The acrylic sheet was bonded to the model structure with epoxy resin and sealed with waterproof tape. It could prevent water and sand from flowing into the model structure.

2.3. Sensor layout and model preparation

According to previous research, the geological structure of the island reef is divided into two layers: an upper layer of coral sand about 17 m thick and a lower reef limestone layer (Wang et al., 2021). Therefore, the model was divided into two layers. Because the compressive strength, elastic modulus, and density of C15 concrete are close to those of reef limestone (Wang, 2008). The lower reef limestone layer was simulated with a C15 concrete slab.

To compare the similarities and differences in the seismic response of the underground structure at the two sites, the excess pore pressure, acceleration, displacement, and dynamic soil pressure of the structure were measured in the tests. Fig. 2 shows the soil profile and sensor

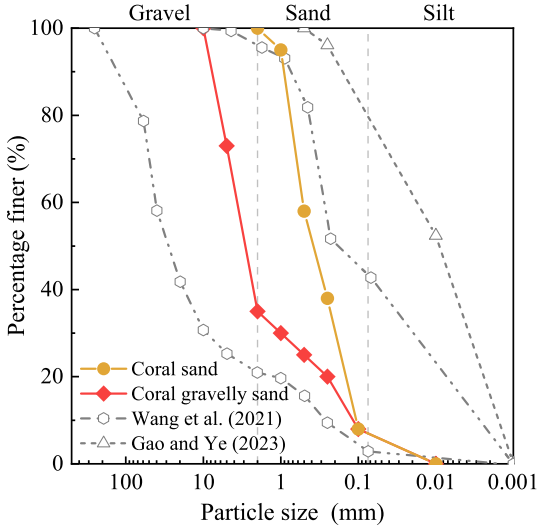

Fig. 1. The grain size distribution curves.

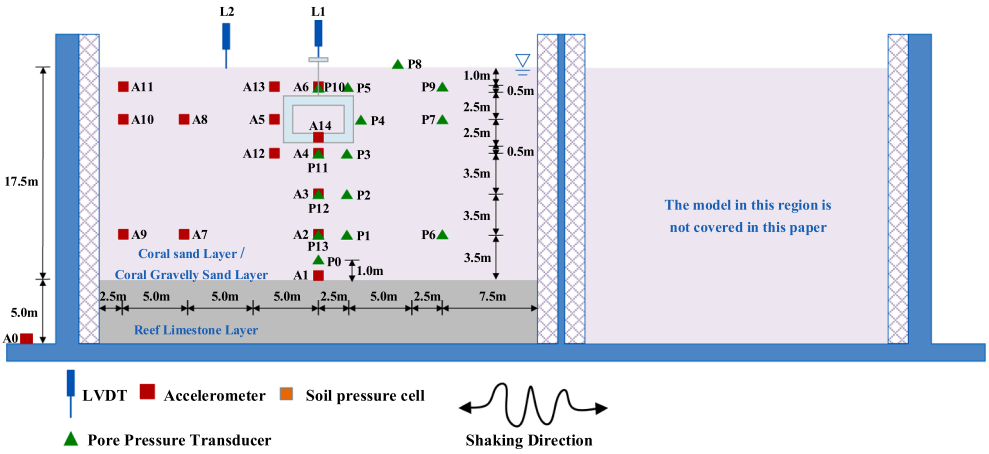

(a) Soil profile

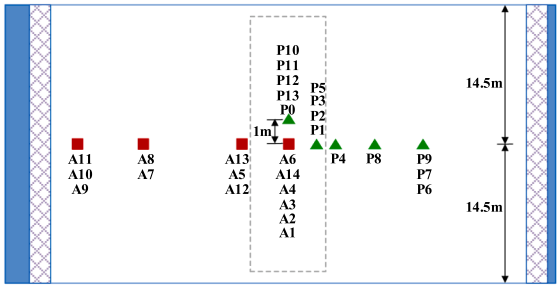

(b) Top view

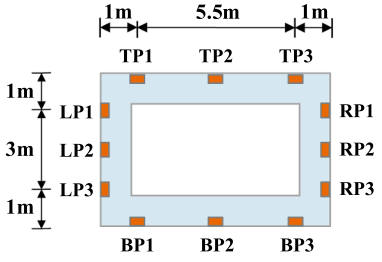

(c) Structural profile

(d) Structural model

Fig. 2. Soil profile and sensor layout (in prototype scale).

Table 2
The scaling laws for dynamic centrifuge modeling.

Types	Physical quantity	Dimensions	Model/Prototype
Geometry properties	Length	L	1/50
Material property	Density	ML^{-3}	1
	Elastic modulus	$ML^{-1}T^{-2}$	1
	Stress	$ML^{-1}T^{-2}$	1
	Strain	–	1
Dynamics Properties	Acceleration	LT^{-2}	50
	Velocity	LT^{-1}	1
	Displacement	L	1/50
	Time (dynamic)	T	1/50
	Time (consolidation)	T	$1/50^2$
	Frequency	T^{-1}	50

Table 3
Physical parameters of the coral gravelly sand and coral sand.

Model	D_r	D_{10} (mm)	D_{50} (mm)	Minimum dry density ρ_{min}(g/cm^3)	Maximum dry density ρ_{max}(g/cm^3)
Coral sand	50 %	0.110	0.400	1.312	1.709
Coral gravelly sand	50 %	0.125	3.184	1.205	1.733

layout of the models. Due to article length constraints, the study of the model on the right side of the container was not covered in this paper. The sensors employed in the tests include fourteen pore pressure transducers, two linear variable differential transformers, fifteen accelerometers, and twelve soil pressure cells, denoted as P, L, A and TP(BP, LP and RP), respectively. P8 was used to monitor the pore pressure of the ground surface. P6, P7 and P9 were used to measure the pore pressure of the far-field soil. The other pore pressure transducers were employed to record the pore pressure of the near-field soil. L1 and L2 were installed to measure the vertical displacement of the structure and ground surface, respectively. A0 was installed to measure the input ground motions. A7-A11 were used to monitor the boundary effect. A14 was employed to record the horizontal acceleration of the underground

structure. The other acceleration transducers were used to measure the acceleration of the near-field soil. Notably, as shown in Fig. 2(c) and (d), grooves were pre-machined on the surface of the structure to facilitate the installation of soil pressure gauges and the burying of wires. The soil pressure gauges were embedded in the surface of the structure, ensuring a more accurate measurement of dynamic soil pressure.

To ensure model uniformity, the model was layered to prepare within the height range based on the model height and sensor positions during model construction. In addition, the target relative density of 50 % was guaranteed by controlling the mass of each soil layer. The mass of the layered coral sand was calculated based on the container's geometric dimensions and target relative density, configured according to the grain size distribution curves. The hydroxypropyl methylcellulose (HPMC) solution with a viscosity of 50 times that of water was used as the pore fluid to satisfy a constant scaling for dynamic time and consolidation time in the tests (Adamidis and Madabhushi, 2015). The prepared model was placed in a vacuum container, which was continuously evacuated by a vacuum pump. To avoid disturbing the model soil, a lower saturation speed was controlled. The saturation of the models was confirmed by the mass of the solution utilized being identical to the theoretical value.

2.4. Input motions and test cases

Fig. 3 shows the acceleration time histories, Arias intensity, and Fourier spectrums of the input motions. The Motion1 was recorded by the K-net submarine station KNG204 during the 2011 Great East Japan earthquake, and the Motion2 was recorded by station KNG205 during the 2006 East Coast of Izu Peninsula earthquake. As shown in Fig. 3, the Motion1 is characterized by abundant long-period components and long duration, and the Motion2 is dominated by short-period components. The Arias intensity represents the overall energy released by seismic motions, integrating the amplitude, frequency, and duration of ground motion (Arias A, 1970). It is clear that Motion1 contains more seismic energy than Motion2.

The ground motion sequences are listed in Table 4. The peak acceleration of the two input motions was scaled to 0.1 g, 0.2 g, and 0.3 g, respectively. Before and after each seismic motion, there was a white noise with an amplitude of 0.01 g to obtain the dynamic characteristics of the sites. In addition, to ensure the full dissipation of excess pore pressure, an interval of 20 min was maintained between consecutive excitations.

Table 4
The ground motion sequence.

Shake sequence	Input motion type	Amplitude (g)
1	Motion1	0.10
2	Motion2	0.10
3	Motion1	0.20
4	Motion2	0.20
5	Motion1	0.30
6	Motion2	0.30

Note: Before and after each seismic motion, there was a white noise with an amplitude of 0.01 g.

3. Test results and analysis

The test results are all provided in the prototype scale unless otherwise indicated. The excess pore pressure, accelerations, displacement, and dynamic soil pressure of the underground structure are presented and discussed in the following.

3.1. Excess pore pressure response

Fig. 4 shows the time histories of the excess pore pressure ratios r_u at the two sites under 0.1 g Motion1. Due to the long dissipation time of excess pore pressure in coral sand, only data of 50 s after the shaking is displayed. As shown in Fig. 4, except for P4, the peak values of r_u increased with the decrease in depth in coral sand and coral gravelly sand. However, the increase in $r_{u,\,max}$ (P10-P13) in coral gravelly sand was much less than that in coral sand. In addition, the $r_{u,\,max}$ in coral gravelly sand was lower than that in coral sand at various depths. It can be attributed to gravel grains, which established well-drained channels in coral gravelly sand, ensuring the timely drainage of pore water. At the end of the shaking, the excess pore pressure beneath the underground structure (P11-P13) in coral gravelly sand had completely dissipated, while significant residual excess pore pressure remained in coral sand. However, it is worth noting that the excess pore pressure above the structure (P10) in coral sand exhibited a similar development mode to that in coral gravelly sand. The excess pore pressure dissipated rapidly after reaching its peak. There is one possible explanation for this. For coral sand, due to the presence of the underground structure, the

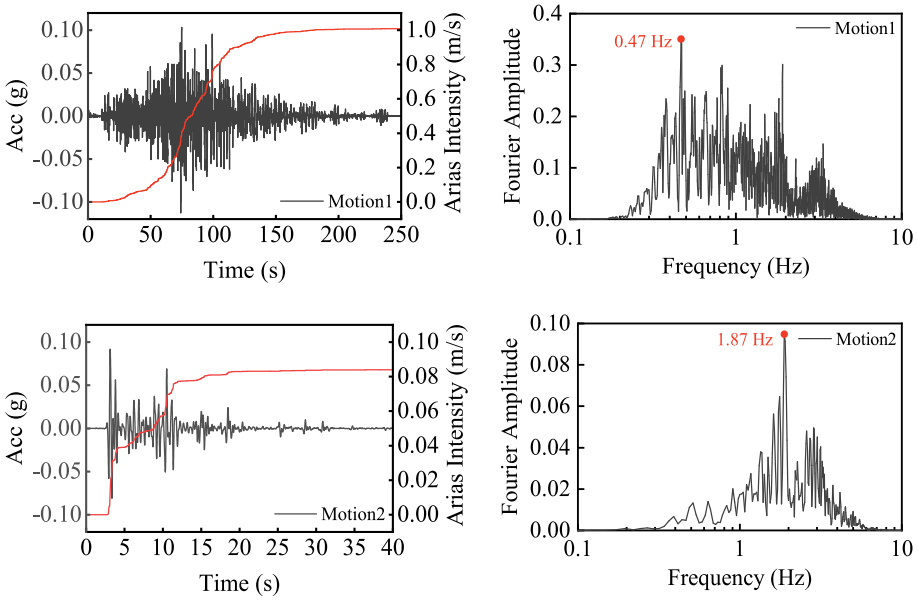

Fig. 3. The acceleration time histories, Arias intensity, and Fourier spectrums of the inputs.

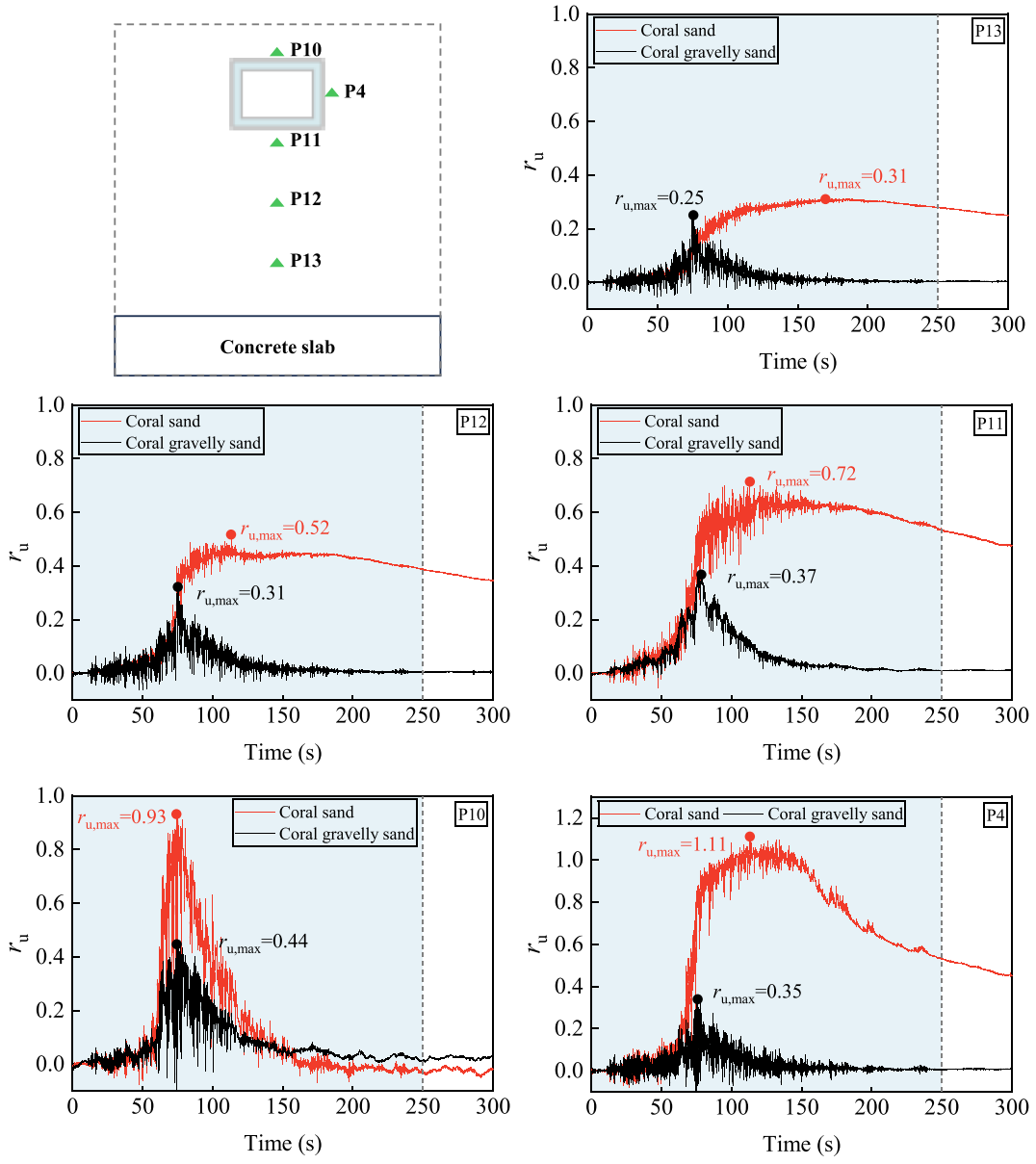

Fig. 4. Time histories of the excess pore pressure ratios in the vertical direction under 0.1 g Motion1.

continuing upward migration of fluid from the deep to the shallow layer was blocked.

The $r_{u,\ max}$ at the side of the structure (P4) reached 1.11 in coral sand, indicating liquefaction of the soil layer, which was significantly higher than that at the bottom of the structure (P11). This phenomenon was also observed in a previous study (An et al., 2021). The contact area between the side wall of the underground structure and the soil formed a drainage channel under the seismic motions. The pore water beneath the structure migrated upward along the drainage channel. Owing to the limited drainage capacity of coral sand, the pore water in the shallow soil (P4) was not promptly discharged and was continuously replenished by the pore water from the lower soil layer, resulting in a higher excess pore pressure ratio at P4. However, the $r_{u,\ max}$ at P4 was slightly lower than that at P11 in coral gravelly sand. Due to the well-drained channels formed by the gravel particles and the shorter drainage path at P4 compared to P11, the $r_{u,\ max}$ at these two positions was similar.

Fig. 5 shows the time histories of the r_u from the two vertical arrays beneath the structure at the two sites under 0.1 g Motion1. One array (P11-P13) was at the center of the structure, and the other array (P1-P3) was at the edge of the structure. As depicted in Fig. 5 (a), the r_u of the two arrays at the same depth almost reached their peaks simultaneously in coral gravelly sand. Furthermore, the $r_{u,\ max}$ near the edge of the bottom of the structure was greater than that at the center of the bottom of the structure. This phenomenon was also observed in a previous study (Chou et al., 2011). However, compared to the center position at the bottom of the structure, there was a time lag when the r_u reached its peak at the edge of the bottom of the structure in coral sand. In addition, the time lag increased with the decrease in the distance from the underground structure. This indicated that the influence of underground structure on the drainage of the foundation in coral sand was greater than that in coral gravelly sand.

The $r_{u,\ max}$ in the vertical direction at the two sites under different intensities of seismic motions are presented in Fig. 6. For coral gravelly sand, the $r_{u,\ max}$ at various depths increased with the intensity of seismic motions and was all less than 1.0, indicating that liquefaction did not occur. In addition, the difference in $r_{u,\ max}$ at different depths was relatively small. However, the liquefaction was observed in coral sand and the liquefaction depth of the soil gradually increased as the intensity

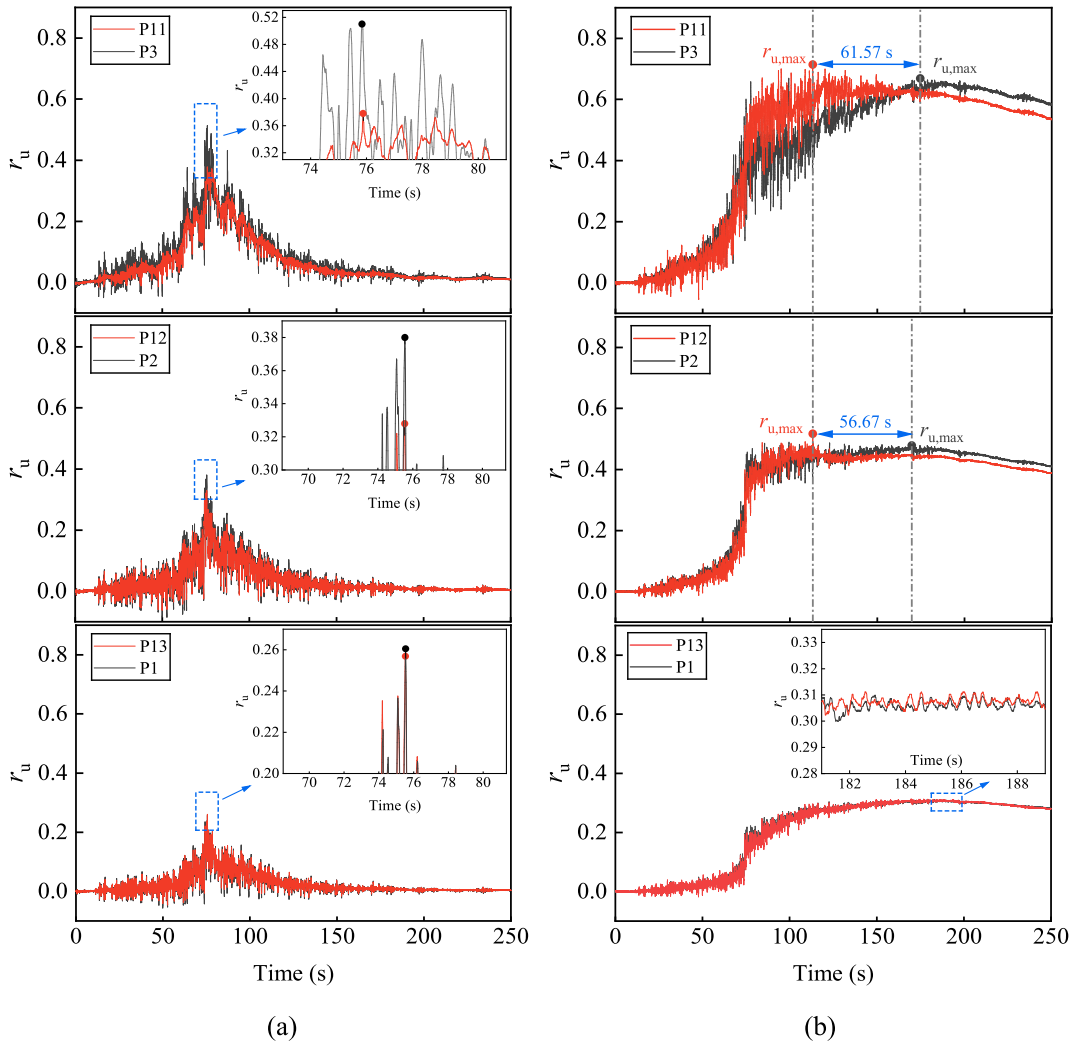

Fig. 5. Time histories of the excess pore pressure ratios from the two vertical arrays beneath the structure at the two sites under 0.1 g Motion1: (a) Coral gravelly sand, (b) Coral sand.

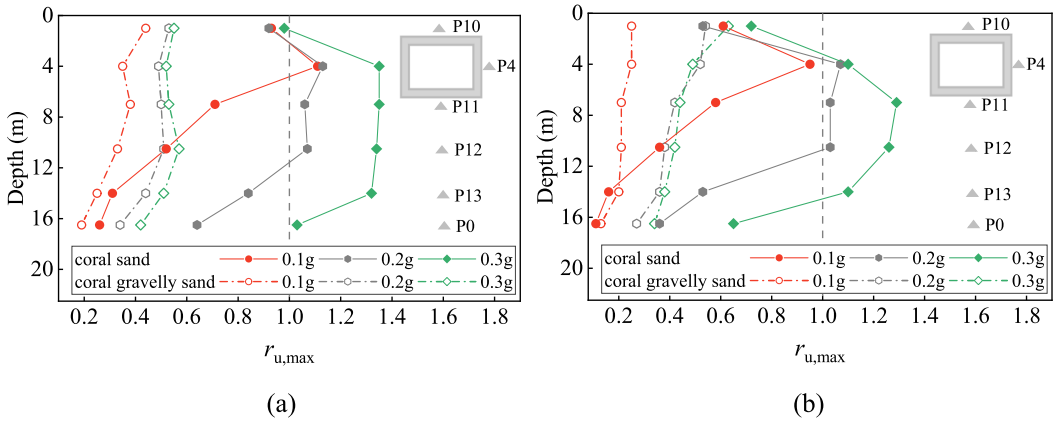

Fig. 6. The $r_{u,\ max}$ in the vertical direction at the two sites under different intensities of seismic motions: (a) Motion1, (b) Motion2.

of seismic motions increased. The soil beneath the underground structure had completely liquefied under the 0.3 g Motion1. Compared to Motion2, Motion1 contained more seismic energy (Fig. 3). Therefore, the $r_{u,\ max}$ at various depths under the Motion1 was larger than that under Motion2 with the same peak acceleration.

The peak values of the differential excess pore pressure between the bottom and top of the underground structure are listed in Table 5. Obviously, the differential excess pore pressure in coral sand was larger than that in coral gravelly sand under the same shaking. For the soil layer under the structure in coral sand, the underground structure restricted the upward discharge of pore water and prolonged the drainage path of pore water, resulting in a continuous increase in excess

Table 5
The peak values of the differential excess pore pressure between the bottom and top of the underground structure (unit: kPa).

Layout of pore pressure transducers	Loading condition	Loading condition					
		Motion1			Motion2		
		0.1 g	0.2 g	0.3 g	0.1 g	0.2 g	0.3 g
▲ P10 ▲ P11	Coral sand	22.7	42.9	46.2	20.1	37.8	43.3
	Coral gravelly sand	8.9	14.0	17.2	5.2	13.2	16.5

pore water pressure. However, due to the well-drained channels, the negative effect of the structure on the action of drainage was small in coral gravelly sand. The peak values of the differential excess pore pressure under the Motion1 were greater than those under the Motion2. There are two possible explanation for this. First, it can be attributed to the longer duration of Motion1, which provided the required time for the higher excess pore pressure accumulation of the soil beneath the structure. In addition, Motion1 contains more seismic energy than Motion2.

3.2. Acceleration response

3.2.1. Acceleration response of the foundation

Fig. 7 shows a comparison of acceleration time histories at the two sites under the 0.1 g Motion1. Due to the malfunction of sensor A5 in coral gravelly sand under the 0.1 g Motion1, the corresponding data was not provided in the figure. The acceleration time histories at deeper depths (A1, A2, A3) were similar at the two sites. As the depth decreased, there were significant differences in the propagation of seismic motion between coral gravelly sand and coral sand. As mentioned above, the $r_{u,\ max}$ at A4 in coral sand was higher than that in coral gravelly sand, implying that the stiffness attenuation in saturated coral sand was more severe. In general, It would weaken the propagation of shear waves. However, the acceleration at A4 in coral sand was significantly greater than that in coral gravelly sand. It could be attributed to the influence of the underground structure. The structure might increase the shear stiffness of the soil. Although the peak value of acceleration at A6 was very close at the two sites, a significant acceleration attenuation was observed in coral sand within about 50 s after reaching the peak acceleration. This was because after reaching the peak acceleration, the soil layer at point A6 in coral sand approached a liquefaction state and the soil severely softened. As a result, it weakened the propagation of seismic motion. This phenomenon also appeared at A13 in coral sand, which was located on the side of the structure and had the same depth as A6, but with a greater degree of attenuation.

The acceleration amplification factors of the model foundation at the two sites under different intensities of seismic motions are presented in Fig. 8. Due to the malfunction of sensor A4 in coral sand under the 0.2 g Motion1 and 0.3 g Motion2, the corresponding data is not provided in the figure. A significant site amplification effect was observed at the two sites under different seismic motions. The site amplification effect basically weakened as the intensity of the seismic motion increased. The amplification factors at A1, A2, and A3 were close between the coral sand and coral gravelly sand. However, the amplification factors near the structure (A4, A6) in coral sand were significantly greater than that in coral gravelly sand under the Motion1. Interestingly, under the Motion2, the acceleration amplification factor at A6 in coral sand was smaller than that in coral gravelly sand, which was contrary to the response under the Motion1. This was because there were differences in the dominant frequency components between Motion1 and Motion2. As shown in Fig. 3, the Motion1 contains a wealth of long-period components, which are dominant in the frequency range. The soil layer at A6 in coral sand was nearly liquefied, which significantly reduced the shear modulus of the soil and enhanced the propagation efficiency of the long-period component of the seismic motion. However, for Motion2, the main seismic energy was concentrated in the high-frequency range and liquefaction attenuated the high-frequency seismic components.

3.2.2. Acceleration response of the underground structure

Fig. 9 shows the acceleration time histories of the underground

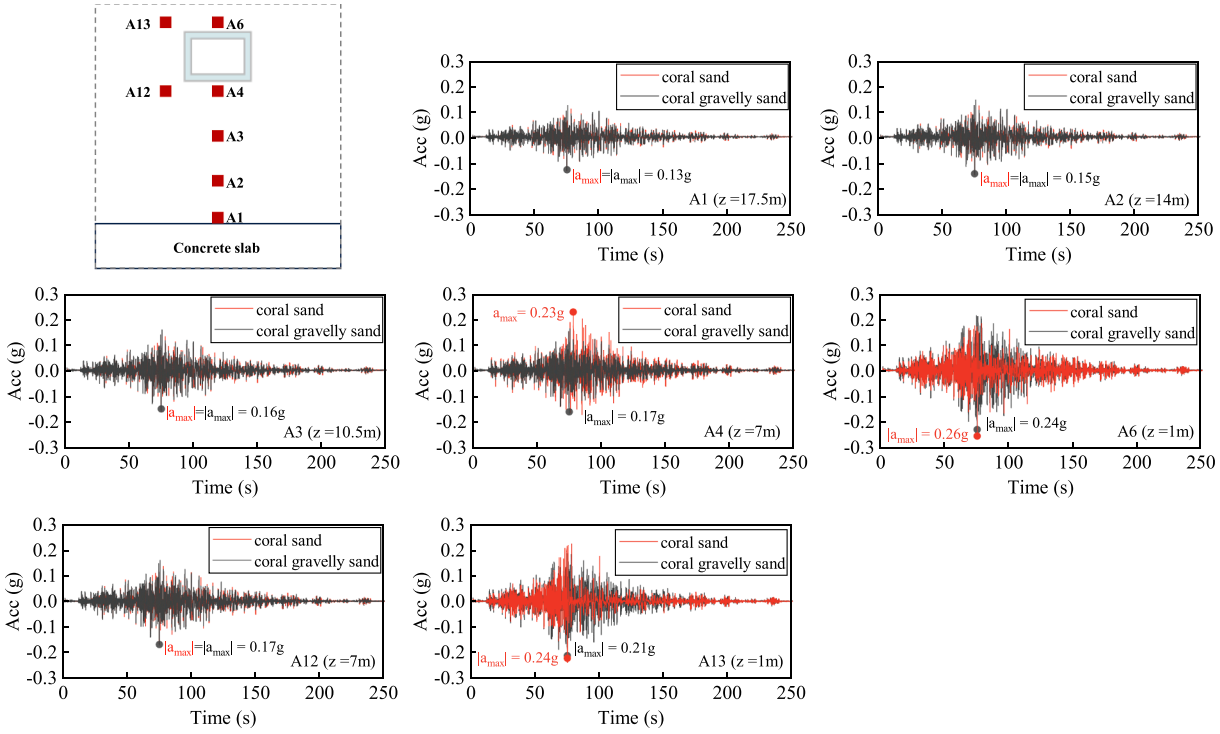

Fig. 7. A comparison of acceleration time histories at the two sites under the 0.1 g Motion1.

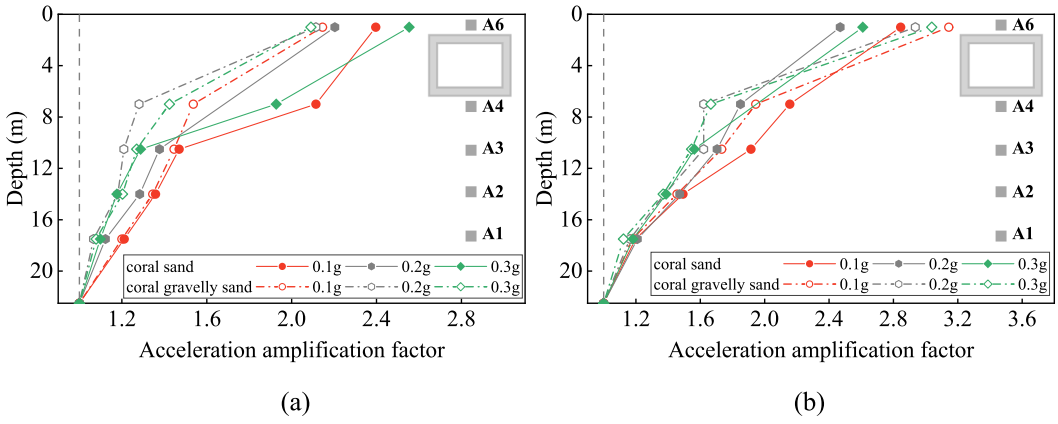

Fig. 8. Acceleration amplification factors of model foundation at the two sites under different intensities of seismic motions: (a) Motion1, (b) Motion2.

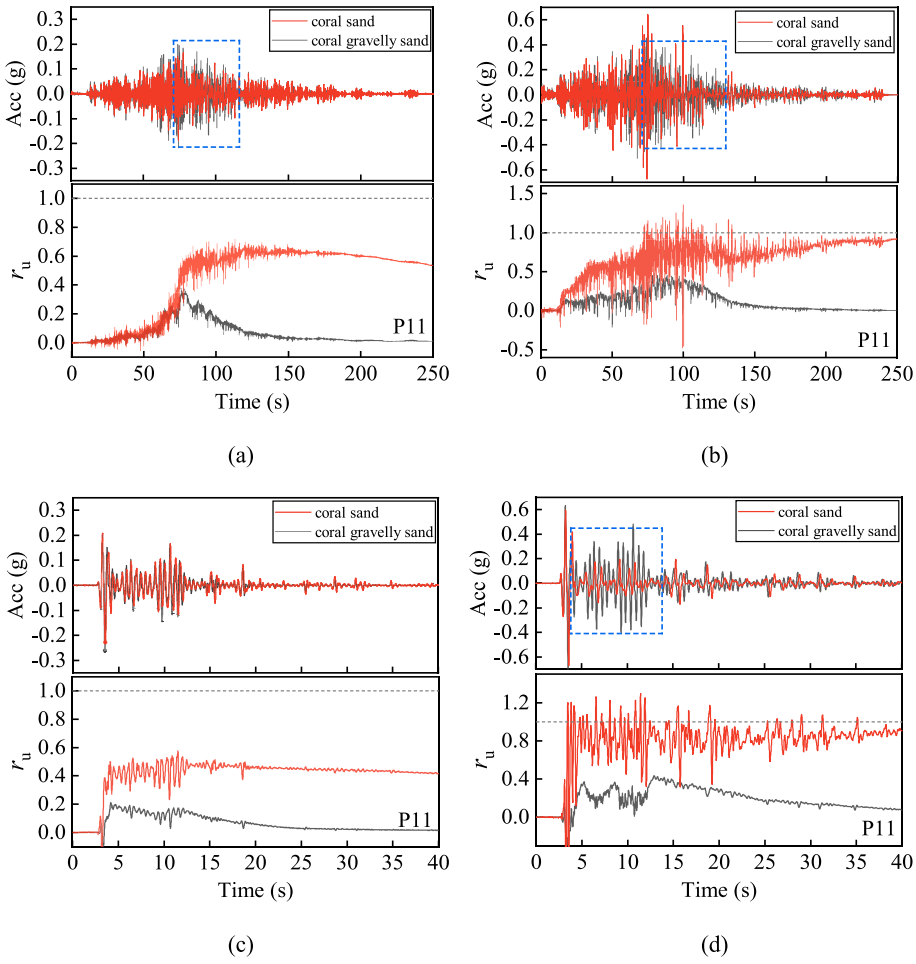

Fig. 9. Acceleration time histories of the underground structure and the r_u at P11 under different seismic motions: (a) 0.1 g Motion1, (b) 0.3 g Motion1, (c) 0.1 g Motion2, and (d) 0.3 g Motion2.

structure under the Motion1 and Motion2. The r_u of the soil layer beneath the structure (P11) is also plotted in the figure. As illustrated in Fig. 9(c), under the ground motion with low intensity, the acceleration response of the underground structure at the two sites was similar, and the response in coral gravelly sand was slightly larger than that in coral sand. However, with the increase in ground motion energy, the excess pore pressure of the soil layer beneath the structure in coral sand gradually increased. Compared to coral gravelly sand, the acceleration of the structure noticeably decreased when the soil layer lost most of its shear stiffness or was completely liquefied (Fig. 9(a), (b), and (d)). This indicated that the acceleration response of the underground structure was closely related to the degree of softening of the soil layer beneath the structure. It can be attributed to the isolation effect of the liquefied soil layer on shear waves. This phenomenon also occurred in a previous experimental study (Chen et al., 2020).

The acceleration response spectra (ARS) 5 % damped of the underground structure under different seismic motions are presented in Fig. 10. The frequency component distributions of the structure's

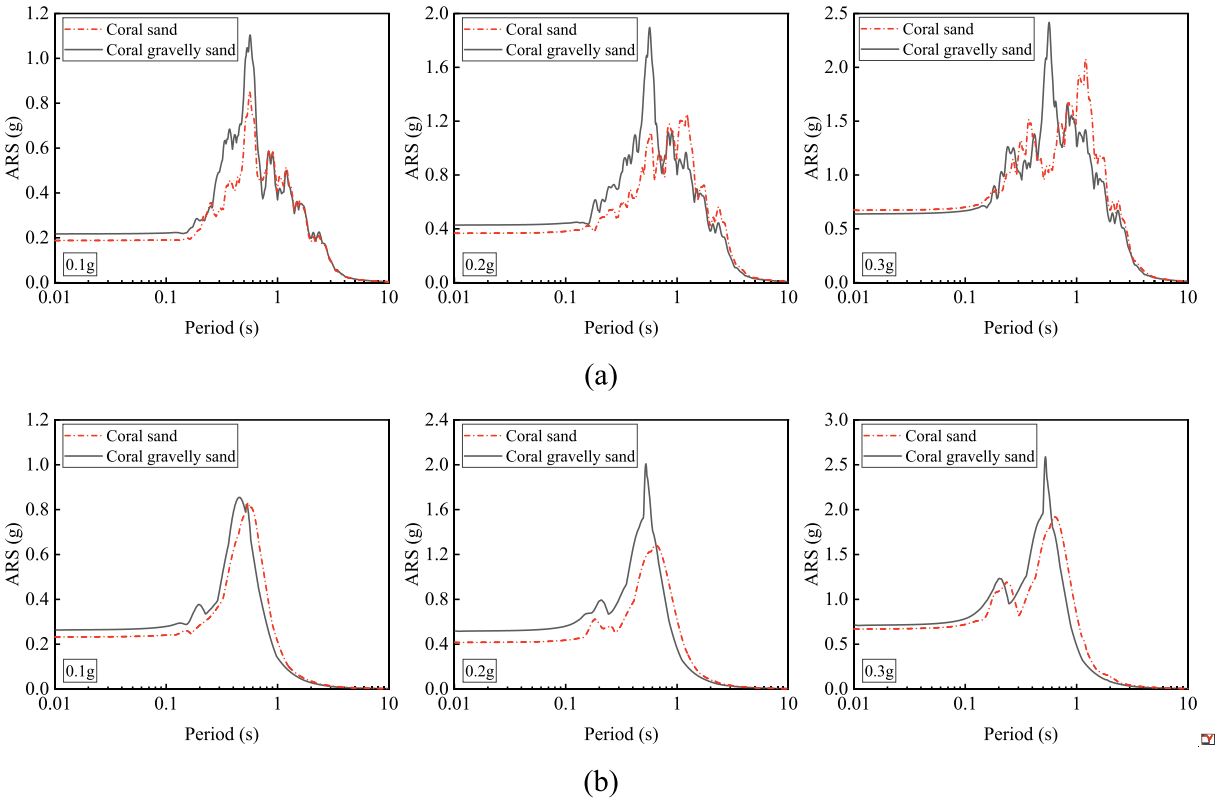

Fig. 10. Acceleration response spectra (ARS) of the underground structure under different seismic motions: (a) Motion1, (b) Motion2.

acceleration were similar at the two sites and the dominant period was near 0.5 s under the 0.1 g Motion1. However, with the increase in seismic intensity, a significant change was observed in the frequency component distribution of the structure's acceleration in coral sand under the Motion1. The dominant period shifted towards the long period (Fig. 10(a)). This was because the soil layer beneath the structure liquefied under strong seismic motions, which amplified the long-period components in the seismic motion and weakened the propagation of

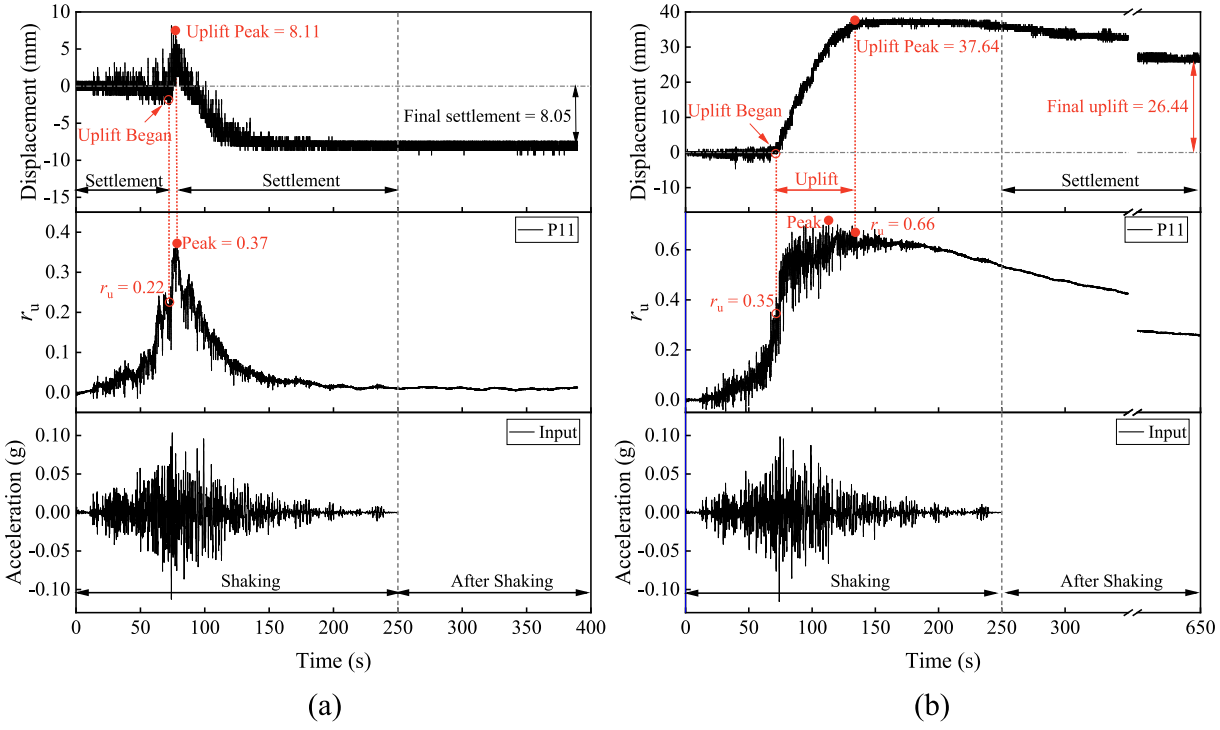

Fig. 11. Relationship among the acceleration, r_u at P11, and movement of the underground structure at the two sites under the 0.1 g Motion1: (a) coral gravelly sand, (b) coral sand.

high-frequency seismic energy. As shown in Fig. 10(b), for the Motion2, the ARS curves of the underground structure at the two sites were similar. It could be attributed to the fact that there were few long-period components in the Motion2. In addition, as the seismic intensity increased, the ARS values of the structure near the dominant period in coral gravelly sand was greater than that in coral sand.

3.3. Displacement response

3.3.1. Vertical displacement of the underground structure

Fig. 11 shows the relationship among the acceleration, r_u at P11, and displacement of the underground structure at the two sites under the 0.1 g Motion1. It was clear that there were significant differences in the development process of vertical displacement of the underground structure in coral sand and coral gravelly sand. The uplift of the structure did not immediately occur when the shaking began, and the displacement of the structure was closely related to the development of excess pore pressure in the soil layer beneath the structure. It was consistent with the law obtained from previous studies (Hu et al., 2018; Fan et al., 2023). For the coral gravelly sand site, the structure exhibited a slight downward movement due to soil densification after the shaking started. The structure gradually floated up as the excess pore pressure accumulated when the r_u of the soil layer beneath the structure reached 0.22. The uplift displacement of the structure and the r_u at P11 reached their peaks simultaneously. Subsequently, a significant subsidence was observed in the structure with the rapid dissipation of the excess pore pressure. At the end of the shaking, the absolute displacement of the structure manifested as settlement and had already reached a stable state. However, for the coral sand site, the structure began to float up when the excess pore pressure ratio at P11 reached 0.35. The uplift of the structure continued after the r_u at P11 reached its peak. The phenomenon was different from that in coral gravelly sand. It could be attributed to the difference in the dissipation pattern of excess pore pressure. The structure slightly moved downward as the excess pore pressure dissipated. At the end of the shaking, the movement of the structure continued due to the large residual excess pore pressure at P11. The absolute displacement of the structure manifested as a significant uplift in coral sand. The same process was also observed in other experiment research (Wang et al., 2022; Fan et al., 2023). Additionally, the uplift displacement of the structure in coral sand was much greater than that in coral gravelly sand during the shaking. It can be concluded that the differences in excess pore pressure development between the two sites led to the differences in the vertical displacement response of the underground structure. Higher excess pore pressure and its longer duration resulted in greater uplift displacement of the underground structure in coral sand.

3.3.2. Macroscopic phenomenon

Fig. 12 shows the macroscopic phenomenon of the displacement response at the two sites. To investigate the differences in seismic responses between the underground structure and the above-ground object, a toy car was placed on the ground. From the macroscopic phenomenon, the underground structure at the two sites floated up while the toy car sank down. This phenomenon was consistent with the results of previous investigations into actual seismic damage at saturated sites (Wakamatsu, 2012). However, the mechanisms causing this macroscopic phenomenon were markedly different between the two sites. Due to the densification of the soil from the shaking, there was a slight downward movement of the toy car with the redistribution of sand beneath at the coral gravelly sand site. But for the coral sand site, the severe sinking of the toy car can be attributed to soil liquefaction, which led to soil softening and a loss of carrying capacity. Fig. 13 presents the foundation settlement and displacement of the underground structure at the two sites. As shown in Fig. 12 and Fig. 13(a), for the coral gravelly sand site, although the macroscopic displacement of the structure manifested as “uplift”, the reason that the elevation of the soil layer above the structure was higher than the surrounding ground was that the absolute settlement of the structure was less than that of the foundation. However, for the coral sand site, the structure continually floated up during the seismic motion, while the foundation settled (Fig. 13(b)).

The relative displacement between the underground structure and the foundation at the two sites under the 0.1 g Motion1 was presented in Fig. 14. It was clear that the relative displacement at the coral sand site was much greater than at the coral gravelly site. Pipeline projects connected to underground structures in coral sand foundations would suffer greater earthquake damage. This provided a reference for practical engineering design.

3.4. Dynamic soil pressure response

Fig. 15 shows the maximum dynamic soil pressure measured in the sidewall at the two sites. It was clear that the dynamic soil pressure increased with the increase in the PGA of input motions. In addition, the distribution pattern of the maximum dynamic soil pressure of the sidewall presented a trapezoidal distribution. The distribution pattern was also observed in previous studies (Watanabe et al., 2016; An et al., 2021; Wang et al., 2022). The maximum dynamic soil pressure in coral sand was greater than in coral gravelly sand under the same seismic motion. It could have been caused by the differences in the development of excess pore pressure on the sides of the structure at the two sites during the shaking. Fig. 16 presents the dynamic soil pressure on the sidewall and the development of excess pore pressure near the sidewall. Interestingly, the development of the dynamic soil pressure was highly similar to that of the excess pore pressure, indicating that the excess pore pressure was one of the main factors contributing to the development of dynamic soil pressure. Additionally, at the end of shaking, the residual dynamic soil pressure remained high in coral sand, whereas the dynamic soil pressure in coral gravelly sand was close to zero. It could potentially lead to greater seismic damage to the underground structure in coral sand.

The difference in dynamic soil pressure between the bottom and the top of the structure is one of the main causes of vertical displacement of underground structures at saturated sites (Chen et al., 2015; An et al.,

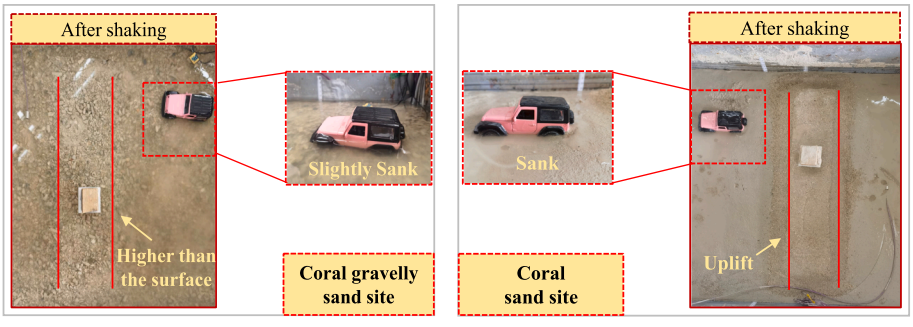

Fig. 12. Macroscopic phenomenon of the displacement response at the two sites.

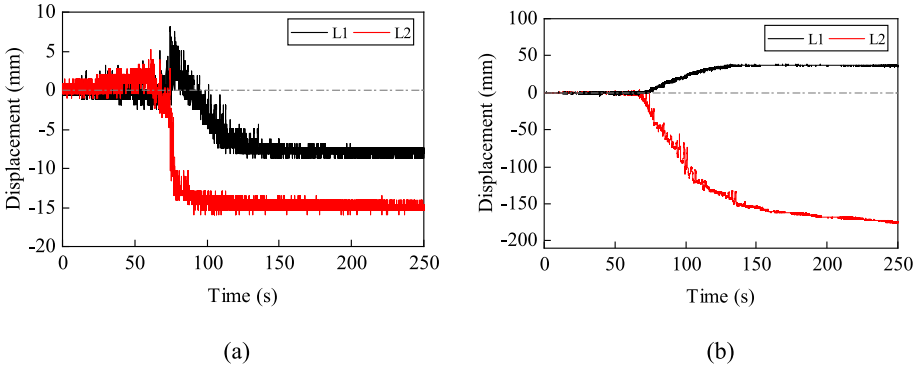

Fig. 13. Foundation settlement (L2) and displacement of underground structure (L1) at the two sites: (a) coral gravelly sand site, and (b) coral sand site.

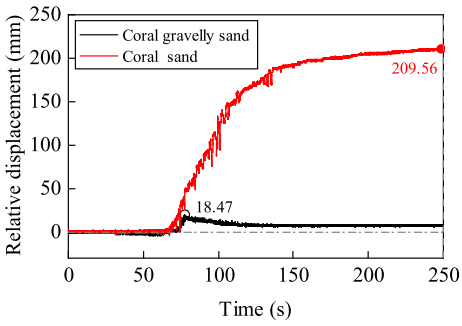

Fig. 14. Relative displacement between the underground structure and the foundation at the two sites under the 0.1 g Motion1.

2021). The peak values of the differential dynamic soil pressure between the bottom and top of the underground structure at the two sites are listed in Table 6. The differential values increased with the intensity of the seismic motion. Comparing the peak values of the differential dynamic soil pressure under the Motion1 and Motion2 with the same PGA, it can be found that the differential value was greater under the Motion1. This was because the Motion1 contained more seismic energy. Furthermore, the differential dynamic soil pressure in coral sand was larger than that in coral gravelly sand under the same shaking, which could lead to a larger uplift displacement of the underground structure.

4. Conclusions

In this study, two centrifuge shaking table tests were conducted to investigate the seismic response of a shallow buried underground structure in saturated coral sand and coral gravelly sand. The similarities and differences in the dynamic behavior of the underground structure at the two sites were analyzed in detail. The main findings were as follows:

(1) The presence of the underground structure significantly affected the development of excess pore pressure in the soil layers around the structure in coral sand. Due to the structure's isolation effect on the pore water below it, the excess pore pressure in the soil layer above the structure quickly dissipated after reaching its peak. However, for the coral gravelly sand, due to the well-drained channels formed by gravel particles, the structure had a small effect on the drainage action during the shaking. Under the same seismic motion, the r_u at various depths in coral sand was greater than that in coral gravelly sand, especially in the positions around the structure. Liquefaction occurred in the soil layer around the structure in coral sand, but it did not occur in coral gravelly sand.

(2) Due to the influence of the structure, the acceleration response of the foundation near the bottom of the structure in coral sand was greater than that in coral gravelly sand. Compared to coral gravelly sand, the acceleration of the soil above the structure in coral sand exhibited a significant attenuation after reaching its peak, which was caused by soil liquefaction. Furthermore, a significant site amplification effect was observed at the two sites. As the intensity of seismic motion increased, the site amplification effect diminished.

(3) The acceleration response of the underground structure was closely related to the development of excess pore pressure in the soil layer at the bottom of the structure. The acceleration response of the underground structure at the two sites was very similar when the excess pore pressure of the soil below the structure was small. However, for the coral sand site, with the increase of seismic intensity, the acceleration of the structure was significantly attenuated and the dominant period shifted towards the long period due to the filtering effect of the soil liquefaction at the bottom of the structure.

(4) There were significant differences in the development process of vertical displacement of the underground structure at the two

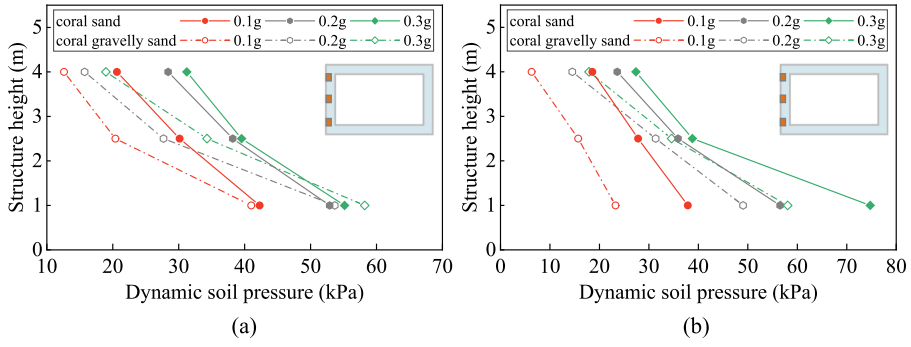

Fig. 15. Maximum dynamic soil pressure on the sidewall of the structure at the two sites: (a) Motion1, (b) Motion2.

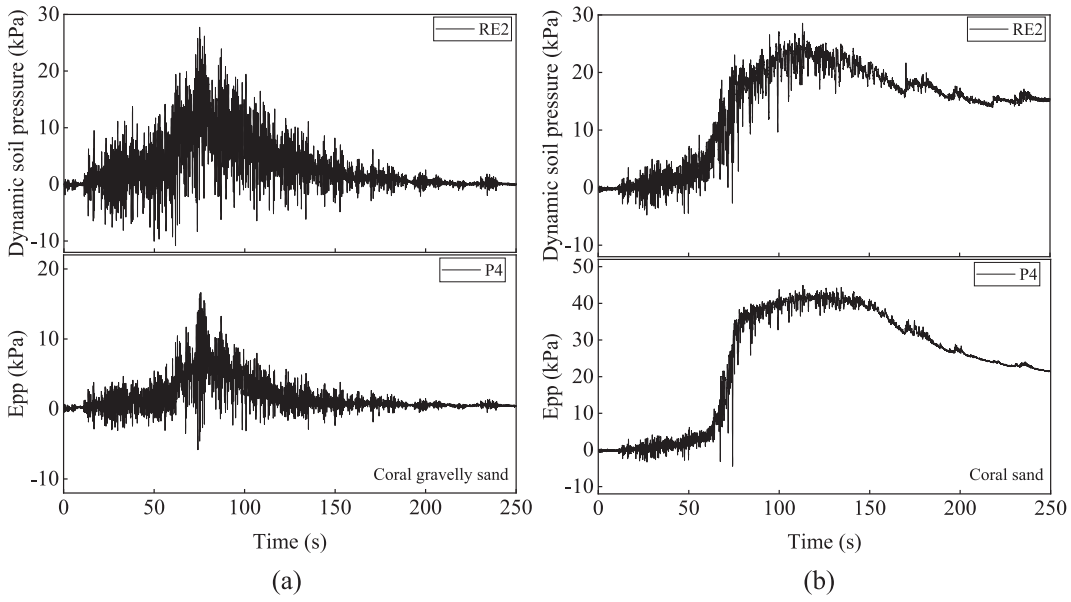

Fig. 16. The relationship between dynamic soil pressure and excess pore pressure (Epp): (a) coral gravelly sand, (b) coral sand.

Table 6
The peak values of the differential dynamic soil pressure between the bottom and top of the underground structure (unit: kPa).

Layout of soil pressure transducers	Loading condition	Loading condition					
		Motion1			Motion2		
		0.1 g	0.2 g	0.3 g	0.1 g	0.2 g	0.3 g
TP2 / BP2	Coral sand	14.2	28.4	48.4	18.1	21.8	34.1
	Coral gravelly sand	6.8	14.1	25.9	4.8	11.4	20.2

sites. The underground structure in coral sand had significantly uplifted under the seismic motions. However, in coral gravelly sand, the displacement mode of the structure was slight subsidence-slight uplift-significant subsidence, and the absolute displacement of the structure was subsidence at the end of the shaking. From the macroscopic phenomenon, the soil layer above the structure was higher than the surrounding ground, which was due to the fact that the settlement of the structure was less than that of the surrounding foundation.

(5) For the sidewalls of the structure, the distribution pattern of the maximum dynamic soil pressure exhibited a trapezoidal distribution and the maximum dynamic soil pressure in coral sand was larger than in coral gravelly sand under the same shaking. In addition, the development of the dynamic soil pressure was closely related to the development of excess pore pressure. Compared to coral gravelly sand, the larger differential dynamic soil pressure between the bottom and top of the underground structure caused the greater uplift displacement of the structure in coral sand.

CRediT authorship contribution statement

Zhongxiang Zhang: Writing – original draft, Visualization, Validation, Investigation, Formal analysis. **Su Chen:** Writing – review & editing, Methodology, Conceptualization. **Yongzhi Wang:** Writing – review & editing, Data curation. **Xiaojun Li:** Writing – review & editing, Supervision, Resources.

Declaration of competing interest

The authors declare that they have no known competing financial interests or personal relationships that could have appeared to influence the work reported in this paper.

Acknowledgments

This work is under the support of the National Natural Science Foundation of China (Grant Numbers 51878626 and 52192675).

Data availability

Data will be made available on request.

References

Adamidis, O., Madabhushi, G.S.P., 2015. Use of viscous pore fluids in dynamic centrifuge modelling. Int. J. Phys. Modell. Geotechn. 15, 141–149. https://doi.org/10.1680/jphmg.14.00022.

An, J., Tao, L., Jiang, L., Yan, H., 2021. A shaking table-based experimental study of seismic response of shield-enlarge-dig type's underground subway station in liquefiable ground. Soil Dyn. Earthq. Eng. 147, 106621.

Arias, A., 1970. A measure of earthquake intensity. MIT Press 438–483.

ASTM, 2016a. D4253-14: Standard test Methods For Maximum Index Density and Unit Weight of Soils Using a Vibratory Table.

ASTM, 2016b. D4254-14: Standard test Methods For Minimum Index Density and Unit Weight of Soils and Calculation of Relative Density.

Burke, L.M., Reytar, K., Spalding, M.D., Perry, A.L., 2011. Reefs at Risk Revisited.

Chen, G., Chen, S., Qi, C., Du, X., Wang, Z., Chen, W., 2015. Shaking table tests on a three-arch type subway station structure in a liquefiable soil. B Earthq Eng 13, 1675–1701.

Chen, S., Tang, B., Zhao, K., Li, X., Zhuang, H., 2020. Seismic response of irregular underground structures under adverse soil conditions using shaking table tests. Tunn. Undergr. Space Technol. 95, 103145. https://doi.org/10.1016/j.tust.2019.103145.

Chinese Ministry of Water Resources, 2007. Standard for engineering classification of soil (GB/T50145-2007) (in Chinese).

Chock, G., Kindred, T., Robertson, I., Iinuma, G., Nicholson, P., Lau, E., Brandes, H., Sarwar, A., Medley, E., Pino, J., Okubo, P., Holmes, W., Hirshorn, B., Sumada, J., 2006. Compilation of Observations of the. Earthquakes, Hawai'i and Mahukona (Mw 6.0.

Chou, J.C., Kutter, B.L., Travasarou, T., Chacko, J.M., 2011. Centrifuge Modeling of Seismically Induced Uplift for the BART Transbay Tube. J Geotech Geoenviron 137, 754–765.

Ding, X., Zhang, Y., Wu, Q., Chen, Z., Wang, C., 2021. Shaking table tests on the seismic responses of underground structures in coral sand. Tunn Undergr Sp Tech 109, 103775.

Ding, X., Zhang, Y., Wu, Q., Cao, G., Chen, Z., 2022. Effects of groundwater level on the seismic responses of coral sand ground and superstructure by shaking table tests. Acta Geotech. 17, 3047–3066. https://doi.org/10.1007/s11440-021-01404-5.
Evans, M.D., Zhou, S., 1995. Liquefaction behavior of sand-gravel composites. J. Geotech. Eng. 121, 287–298.
Fan, J., Zhao, X., Liu, J., Huang, B., 2023. Seismic response of buried pipes in sloping medium dense sand. Soil Dyn Earthq Eng 170, 107867.
Gao, R., Ye, J., 2023. Mechanical behaviors of coral sand and relationship between particle breakage and plastic work. Eng. Geol. 316, 107063.
Ghasemi, H., Cooper, J.D., Imbsen, R.A., Piskin, H., Inal, F., Tiras, A., 2000. The November 1999 Duzce Earthquake: post-earthquake investigation of the structures on the TEM. United States, Federal Highway Administration.
Green, R.A., Olson, S.M., Cox, B.R., Rix, G.J., Rathje, E., Bachhuber, J., French, J., Lasley, S., Martin, N., 2011. Geotechnical Aspects of Failures at Port-au-Prince Seaport during the 12 January 2010 Haiti Earthquake. Earthq. Spectra 27, 43–65.
Hazarika, H., Kokusho, T., Kayen, R., Dashti, S., Fukuoka, H., Ishizawa, T., Kochi, Y., Matsumoto, D., Furuichi, H., Hirose, T., others, 2017. Geotechnical damage due to the 2016 Kumamoto Earthquake and future challenges. lowland technology international 19, 203–218.
Hu, J., Chen, Q., Liu, H., 2018. Relationship between earthquake-induced uplift of rectangular underground structures and the excess pore water pressure ratio in saturated sandy soils. Tunn. Undergr. Space Technol. 79, 35–51.
Hubler, J., 2017. Laboratory and in-situ assessment of liquefaction of gravelly soils. University of Michigan, AnnArbor. PhD Thesis.
Iida, H., Hiroto, T., Yoshida, N., Iwafuji, M., 1996. Damage to Daikai subway station. Soils Found. 36, 283–300.
Liu, H., Zhang, J.-M., Zhang, X., Wang, R., 2020. Seismic performance of block-type quay walls with liquefiable calcareous sand backfill. Soil Dyn. Earthq. Eng. 132, 106092. https://doi.org/10.1016/j.soildyn.2020.106092.
Mejia, Y., 1995. Liquefaction of coralline soils during the 1993 Guam earthquake. San Diego, USA.
Moss, R.E., Thompson, E.M., Scott Kieffer, D., Tiwari, B., Hashash, Y.M., Acharya, I., Adhikari, B.R., Asimaki, D., Clahan, K.B., Collins, B.D., et al., 2015. Geotechnical effects of the 2015 magnitude 7.8 Gorkha, Nepal, earthquake and aftershocks. Seismol. Res. Lett. 86, 1514–1523.
Olson, S.M., Green, R.A., Lasley, S., Martin, N., Cox, B.R., Rathje, E., Bachhuber, J., French, J., 2011. Documenting Liquefaction and Lateral Spreading Triggered by the 12 January 2010 Haiti Earthquake. Earthq. Spectra 27, 93–116. https://doi.org/10.1193/1.3639270.
Ruttithivaphanich, P., Sasanakul, I., 2022. Centrifuge modeling studies on effects of composition on liquefaction of mine waste rock. Soil Dyn Earthq Eng 160, 107378.
Sengupta, D., Chen, R., Meadows, M.E., 2018. Building beyond land: An overview of coastal land reclamation in 16 global megacities. Appl. Geogr. 90, 229–238.
Wakamatsu, K., 2012. Recurrence of liquefaction at the same site induced by the 2011 Great East Japan Earthquake compared with previous earthquakes, in: 15th World Conference on Earthquake Engineering (15WCEE), Lisbon.
Wang, X., Ding, H., Meng, Q., Wei, H., Wu, Y., Zhang, Y., 2021. Engineering characteristics of coral reef and site assessment of hydraulic reclamation in the South China Sea. Constr. Build. Mater. 300, 124263. https://doi.org/10.1016/j.conbuildmat.2021.124263.
Wang, Z., Gao, B., Jiang, Y., Yuan, S., 2009. Investigation and assessment on mountain tunnels and geotechnical damage after the Wenchuan earthquake. Sci. China Ser. E: Technol. Sci. 52, 546–558.
Wang, X., Liu, J.-Q., Cui, J., Wang, X.-Z., Shen, J.-H., Zhu, C.-Q., 2021. Particle breakage characteristics of a foundation filling material on island-reefs in the South China Sea. Constr. Build. Mater. 306, 124690.
Wang, W., Wang, T., Su, J., Lin, C., Seng, C., Huang, T., 2001. Assessment of damage in mountain tunnels due to the Taiwan Chi-Chi Earthquake. Tunn. Undergr. Space Technol. 16, 133–150.
Wang, X., Yang, X., Zeng, X., 2017. Seismic centrifuge modelling of suction bucket foundation for offshore wind turbine. Renew Energ 114, 1013–1022.
Wang, J., Yang, J., Zhuang, H., Ma, G., Sun, Y., 2022. Seismic Responses of a Large Unequal-span Underground Subway Station in Liquefiable Soil Using Shaking Table Test. J Earthq Eng 26, 8446–8467. https://doi.org/10.1080/13632469.2021.1991523.
Xinzhi Wang, 2008. Study on Engineering Geological Properties of Coral reefs and Feasibility of Large Project Construction on Nansha Islands (PhD thesis). Institute of Rock and Soil Mechnics. The Chinese Academy of Sciences, Wuhan, China.
Watanabe, K., Sawada, R., Koseki, J., 2016. Uplift mechanism of open-cut tunnel in liquefied ground and simplified method to evaluate the stability against uplifting. Soils Found. 56, 412–426. https://doi.org/10.1016/j.sandf.2016.04.008.
Wham, B., Dashti, S., Franke, K., Kayen, R., Oettle, N., 2017. Water supply damage caused by the 2016 Kumamoto Earthquake. Lowland Technology International 19, 151–160.
Wu, Q., Ding, X., Chen, Z., Zhang, Y., 2020. Shaking Table Tests on Seismic Responses of Pile-soil-superstructure in Coral Sand. J Earthq Eng 1–27.
Wu, Q., Ding, X., Zhang, Y., Chen, Z., Zhang, Yu., 2021. Numerical simulations on seismic response of soil-pile-superstructure in coral sand. Ocean Eng. 239, 109808. https://doi.org/10.1016/j.oceaneng.2021.109808.
Wu, Q., Ding, X., Zhang, Y., Zhang, Y., 2023. Numerical analysis of seismic response of rectangular underground structure in coral sand. Underground Space 9, 155–172.
Wu, Q., Ding, X., Zhang, Y., Xin, Y., 2024. Experimental and Numerical Study on Dynamic Response of Underground Structure in Coral Sand Under Earthquakes. J. Earthq. Eng. 28, 62–84. https://doi.org/10.1080/13632469.2023.2173491.
Xie, X., Ye, B., Zhao, T., Feng, X., Zhang, F., 2021. Changes in sand mesostructure under repeated seismic liquefaction events during centrifuge tests. Soil Dyn. Earthq. Eng. 150, 106940. https://doi.org/10.1016/j.soildyn.2021.106940.
Xu, D., Liu, H., Rui, R., Gao, Y., 2019. Cyclic and postcyclic simple shear behavior of binary sand-gravel mixtures with various gravel contents. Soil Dyn. Earthq. Eng. 123, 230–241.
Yamaguchi, A., Mori, T., Kazama, M., Yoshida, N., 2012. Liquefaction in Tohoku district during the 2011 off the Pacific Coast of Tohoku Earthquake. Soils Found. 52, 811–829.
Yu, H., Zeng, X., Li, B., Lian, J., 2015. Centrifuge modeling of offshore wind foundations under earthquake loading. Soil Dyn. Earthq. Eng. 77, 402–415.
Yuan, X., Zhang, W., Duan, Z., Sun, R., Wang, Y., Zhang, W., 2019. Analysis for characteristics of seismic liquefaction in engineering sites of coralline soils. Chin. J. Rock Mech. Eng. 38, 3799–3811.
Zhang, Y., He, K., Li, X., Ye, J., 2022. Centrifuge Shaking Table Test on the Seismic Dynamics of Revetment Breakwater and a Nearby Aircraft Runway Built on Reclaimed Coral Sand Foundation. J Mar Sci Eng 11, 41. https://doi.org/10.3390/jmse11010041.
Zhou, Y.-G., Sun, Z.-B., Chen, Y.-M., 2018. Zhejiang University benchmark centrifuge test for LEAP-GWU-2015 and liquefaction responses of a sloping ground. Soil Dyn Earthq Eng 113, 698–713. https://doi.org/10.1016/j.soildyn.2017.03.010.